Fundamental Thickness Limit of Itinerant Ferromagnetic SrRuO$_3$ Thin Films

Young Jun Chang,[1] Choong H. Kim,[2] S.-H. Phark,[1] Y. S. Kim,[1] J. Yu,[2] and T. W. Noh[1,*]

[1]*ReCOE & FPRD, Department of Physics and Astronomy, Seoul National University, Seoul 151-747, Korea*
[2]*CSCMR & FPRD, Department of Physics and Astronomy, Seoul National University, Seoul 151-747, Korea*
(Received 21 February 2009; published 30 July 2009)

We report on a fundamental thickness limit of the itinerant ferromagnetic oxide SrRuO$_3$ that might arise from the orbital-selective quantum confinement effects. Experimentally, SrRuO$_3$ films remain metallic even for a thickness of 2 unit cells (uc), but the Curie temperature T_C starts to decrease at 4 uc and becomes zero at 2 uc. Using the Stoner model, we attributed the T_C decrease to a decrease in the density of states (N_o). Namely, in the thin film geometry, the hybridized Ru $d_{yz,zx}$ orbitals are terminated by top and bottom interfaces, resulting in quantum confinement and reduction of N_o.

SrRuO$_3$ is an itinerant ferromagnetic oxide with a ferromagnetic Curie temperature (T_C) of 160 K and a magnetic moment of $1.6\mu_B$ [1,2]. At T_C, its electrical resistivity curve changes slope due to the decrease in spin fluctuations [3]. The ferromagnetic metallic ground state can be understood in the framework of the Stoner model [3], which is based on the competition between the kinetic energy and exchange energy due to Coulomb repulsion. The stabilization of a ferromagnetic state is favored when

$$IN_0 > 1, \qquad (1)$$

where N_0 and I are the nonmagnetic density of state (DOS) at the Fermi level E_F and the effective electron-electron interaction, respectively. The model also predicts that

$$T_C \propto [1 - 1/(IN_0)]^{1/2}. \qquad (2)$$

Note that a systematic variation of N_0 can induce T_C change in the band ferromagnetic material.

In simple metals, ultrathin films are known to exhibit quantum confinement (QC) effects due to the confinement of electrons inside the conducting layers [4]. These effects alter the electronic structure and N_0, so they can result in striking variations of the physical properties such as conductivity, magnetism, and the Hall effect. However, up to this point, no QC effects have been reported in oxide ultrathin films, including SrRuO$_3$.

SrRuO$_3$ is also one of the most frequently used oxide electrode materials. It has high chemical stability, good thermal properties [5], and the perovskite crystal structure, which are advantageous for integration with other oxide materials into heterostructures [6]. SrRuO$_3$ has been used in numerous oxide applications, including Josephson junctions [7], magnetic tunneling junctions [8], Schottky junctions [9], field effect devices [10], ferroelectric capacitors [11,12], and multiferroic devices [13]. To design such oxide thin film devices, it is important to understand how thickness (t) affects the transport and magnetic properties of SrRuO$_3$, especially in the ultrathin limit.

In this Letter, we report on the thickness-dependent ferromagnetism of ultrathin SrRuO$_3$ films. We observed that the metallic properties of SrRuO$_3$ ultrathin films are maintained down to $t = 2$ uc (unit cells), but T_C starts to decrease at $t = 4$ uc and becomes zero at $t = 2$ uc. To explain the T_C reduction, we investigated the variation of N_0 using *in situ* scanning tunneling spectroscopy (STS) and the first-principles calculations. Both of these experimental and theoretical studies showed a significant decrease in the DOS at E_F for $t < 4$ uc. This behavior could be explained in terms of QC of Ru $d_{yz,zx}$ orbitals.

To obtain high-quality SrRuO$_3$ ultrathin films, we used a TiO$_2$-terminated SrTiO$_3$ (001) substrate, the surface of which is atomically flat with 1-uc-high steps (small miscut, i.e., $<0.1°$). On top of the substrate, we deposited SrRuO$_3$ films using pulsed laser deposition (PLD) at 700 °C with an oxygen pressure of 0.1 Torr and a laser fluence of 2.5 J/cm^2 [14]. The growth rate of SrRuO$_3$ films was about 0.015 nm/sec. The film thickness was controlled by *in situ* monitoring of the reflection high-energy electron diffraction intensity oscillation while a two-dimensional (2D) growth mode was maintained. Ambient atomic force microscopy (AFM) topography of the SrRuO$_3$ films shows atomically smooth surfaces that resemble the substrate surface, as shown in Figs. 1(a)–1(c), indicating the step-flow growth mode [15,16].

Figure 1(e) shows the temperature-dependent dc resistivity $\rho(T)$ for SrRuO$_3$ films for various values of t. As t decreases, the $\rho(T)$ curves show systematic changes: namely, the $\rho(20\,\text{K})$ value becomes higher and the slope change occurs at a lower temperature. It should be noted that our SrRuO$_3$ films remain metallic down to $t = 2$ uc. As stated earlier, $\rho(T)$ should show an anomaly at T_C. As indicated by the arrows in Fig. 1(e), the $\rho(T)/\rho(300\,\text{K})$ data also show anomalies, which we attribute to the ferromagnetic ordering. We estimated the T_C values by differentiating the $\rho(T)/\rho(300\,\text{K})$ curves. The black solid circles in Fig. 2(a) show the experimental T_C data for the SrRuO$_3$ films. Above 4 uc, T_C remains nearly constant.
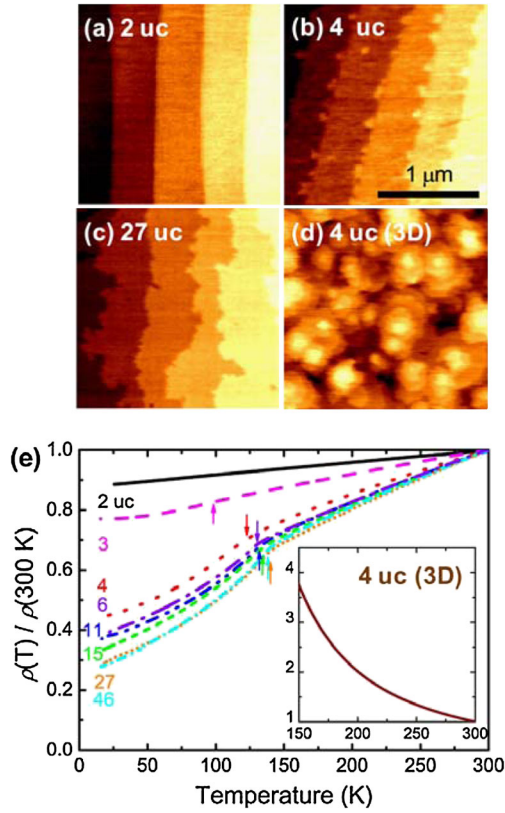
FIG. 1 (color online). (a)–(c) AFM topography of SrRuO$_3$ thin films for different thickness values (t) of (a) 2, (b) 4, and (c) 27 uc. (d) Topography of rough film with $t = 4$ uc obtained from much faster growth rate. All images are 2 μm × 2 μm in size. (e) Temperature (T) dependence of the normalized resistivity $\rho(T)/\rho(300\ \text{K})$ of SrRuO$_3$ thin films for t of 2–46 uc. The SrRuO$_3$ films remain metallic down to 2 uc. The inset shows the $\rho(T)/\rho(300\ \text{K})$ of the rough film with $t = 4$ uc.

However, T_C decreases drastically below 4 uc, and it becomes zero for the 2-uc film.

There have been earlier experimental reports that a metal-insulator transition should occur at either 3 or 4 uc of the SrRuO$_3$ film [17,18]. Note that our observation on the persistence of the metallic state down to 2 uc is not consistent with the earlier experimental reports but agrees with the first-principles calculations [19]. To obtain further insight, we deposited SrRuO$_3$ ultrathin films at a higher growth rate of 0.045 nm/ sec. As shown in Fig. 1(d), the surface morphology of the films is very rough, indicating a 3D island growth mode even for the film with $t = 4$ uc. As shown in the inset in Fig. 1(e), the rough film has an insulating behavior. Therefore, the difference between our work and earlier work could be attributed to the effects of disorder, such as grain boundaries and step edges.

Using our high-quality SrRuO$_3$ thin films, we investigated the thickness dependence of the low temperature resistivity, i.e., $\rho(20\ \text{K})$. Our 46-uc film has $\rho(20\ \text{K}) = 51\ \mu\Omega\,\text{cm}$, which is comparable to its bulk value of 20 $\mu\Omega$ cm [1]. As shown in Fig. 2(b), $\rho(20\ \text{K})$ increases
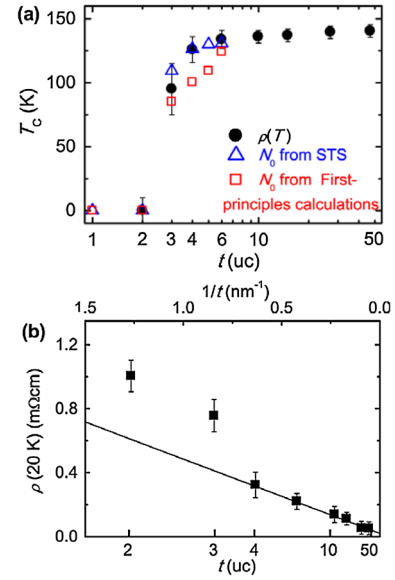

FIG. 2 (color online). (a) t dependence of T_C values. Experimental T_C values (black solid circles) were obtained from the peak T positions in the inset in Fig. 1(b). T_C values were also estimated based on the Stoner model, i.e., Eq. (2), using values for the nonmagnetic density of state at the Fermi level (N_0) estimated from *in situ* STS studies (blue open triangles) and first-principles calculations (red open squares). (b) t dependence of $\rho(20\ \text{K})$. The solid line is the classical theoretical prediction based on the increased surface scattering.

systematically with a decrease in t. According to the Drude model for a metal, $\rho = m^*/ne^2\tau$, where m^*, n, and τ are the effective mass, number density, and scattering time of the free carriers, respectively. Down to 4 uc, the increase in $\rho(20\ \text{K})$ can be explained in terms of the enhanced surface scattering rates in a film geometry. Namely, the effect of t can be incorporated by including an additional channel of scattering at the top and the bottom surfaces of the thin film. According to Matthiessen's rule, the net ρ is described by a combined τ with contributions from the bulk and the surface scattering [20]. Assuming that the surface scattering determines the minimum value of electron collision time in the thin film, we have

$$\rho = \rho_b + \left(\frac{m^* v_F}{ne^2}\right)\frac{1}{t}, \qquad (3)$$

where ρ_b and v_F are the bulk resistivity and the Fermi velocity, respectively. Using the reported bulk values of $\rho_b(20\ \text{K}) \approx 20\ \mu\Omega$ cm, $m^* \approx 7m_e$, $v_F \approx 2 \times 10^7$ cm/s, $n \approx 1.2 \times 10^{22}/\text{cm}^3$, and $\tau \approx 5 \times 10^{-15}$ sec [1,21,22], Eq. (3) describes the t-dependent $\rho(20\ \text{K})$ for our SrRuO$_3$ films with $t > 4$ uc. The solid line in Fig. 2(b) is the classical theoretical prediction based on the increased surface scattering. For the films with $t = 2$ and 3 uc, $\rho(20\ \text{K})$ becomes even higher than the classical predictions. A comparison with Eq. (3) indicates the possibility of decreasing n for $t < 4$ uc.

To obtain experimental evidence of the t-dependent change of N_0, we carried out *in situ* STS studies on 1- to 6-uc-thick SrRuO$_3$ films, which were grown on semiconducting Nb(0.1%)-doped SrTiO$_3$ substrates. Figure 3 shows the tunneling current (I_t) versus tip bias voltage (V_{tip}) at room temperature, obtained in an ultrahigh vacuum scanning tunneling microscopy chamber connected in a vacuum to the PLD system. The red line corresponds to the I_t-V_{tip} spectra of a 50-uc-thick film, which is expected to show nearly the same metallic behavior as the bulk material. As t increases, the corresponding I_t becomes larger at a given V_{tip}. The inset in Fig. 3 shows the tunneling conductance (dI_t/dV_{tip}) values at zero bias, which should be proportional to N_0 [23]. As t decreases, the $dI_t/dV_{tip}(0 \text{ V})$ values decrease monotonically. In particular, the decrease becomes quite significant below 4 uc. In addition, $dI_t/dV_{tip}(0 \text{ V})$ remains finite for the 1-uc film. Using the Stoner theory in Eq. (2), the T_C values were evaluated and plotted as blue triangles in Fig. 2(a). The excellent agreement with the T_C values from the $\rho(T)$ curves indicates that the decrease in N_0 in SrRuO$_3$ ultrathin films should play an important role in their ferromagnetic properties [24].

To understand the thickness dependence of N_0, we carried out first-principles calculations based on the density functional theory using VASP code with the Ceperley-Alder parameterization of the local spin density approximation
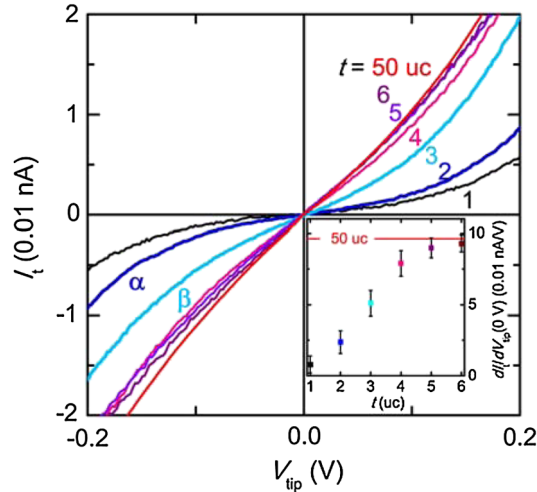
and projector-augmented wave potentials. The cutoff energy for the plane waves was 500 eV. We sampled the k points from the $12 \times 12 \times 1$ Monkhorst-Pack (MP) grid and performed integrations with 0.2 eV Gaussian smearing. To calculate more accurate projected density-of-state (pDOS), we also used the $24 \times 24 \times 1$ MP k-point grid and tetrahedron method. In our calculations, we did not consider the effect of on-site Coulomb interactions. We used 3.5-uc SrTiO$_3$ (4 SrO layers and 3 TiO$_2$ layers) slabs sandwiched symmetrically by 1- to 6-uc SrRuO$_3$ slabs. We fixed the in-plane and out-of-plane lattice constants of the ultrathin films to the experimental values $a = 0.3905$ nm and $c = 0.3959$ nm, respectively.

Figure 4(a) displays schematic pictures of the samples used for the calculations: 1- and 4-uc SrRuO$_3$ films on 2-uc SrTiO$_3$. Initially, we calculated the pDOS for the nonmagnetic ground states of each SrRuO$_3$ layer in the SrRuO$_3$ films with $t = 1$–4 uc. The four gray plots in the middle of Fig. 4(b) show the nonmagnetic pDOS projected onto a layer close to the center of the SrRuO$_3$ thin film. The 1-uc film shows a few sharp peaks around E_F, i.e., near 0 eV. As the film becomes thicker, a larger number of peaks
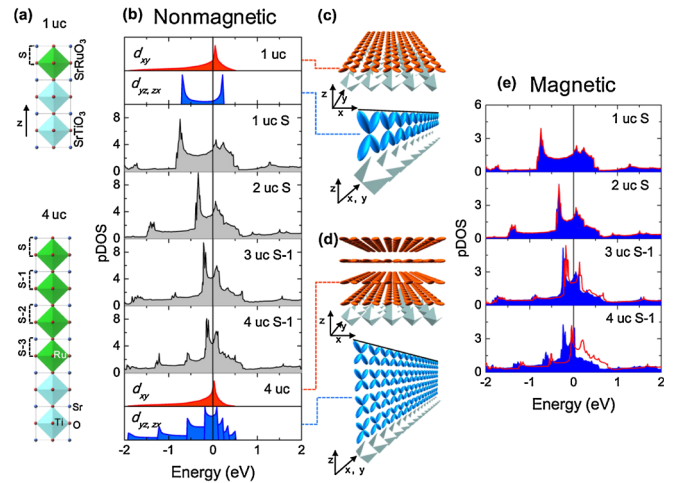

FIG. 4 (color online). (a) Schematic model systems: 1 and 4 uc of SrRuO$_3$ on 2 uc of SrTiO$_3$. The green and blue squares represent the metal-oxygen octahedra with Ru^{4+} and Ti^{4+} ions, respectively. The symbol of S-i indicates the ith SrRuO$_3$ layer from the surface. (b) Calculated nonmagnetic pDOS (gray) for the middle SrRuO$_3$ layer in films with $t = 1$–4 uc. Note that the pDOS at 0 eV decreases with decreasing t. (c) Orbital configurations of the t_{2g} electrons of Ru^{4+} ions in the 1 uc SrRuO$_3$ film. The d_{xy} orbitals (red) are hybridized with the oxygen 2p orbitals (not shown) and form an infinite 2D sheet. On the other hand, because of the truncation in the z direction, the d_{yz} or d_{zx} orbitals (blue) form a 1D strip. The Ti-oxygen octahedra are shown in sky blue. (d) Orbital configurations of the t_{2g} electrons of Ru^{4+} ions in the 4-uc SrRuO$_3$ film. (e) Calculated pDOS with ferromagnetic configurations for the middle SrRuO$_3$ layer in films with $t = 1$–4 uc. The majority and minority spin states are colored in blue (filled) and red (unfilled), respectively.

FIG. 3 (color online). Plot of the tunneling current I_t versus tip bias voltage V_{tip} obtained from SrRuO$_3$ films grown on a Nb-doped SrTiO$_3$ substrate. The inset shows the t dependence of the tunneling conductance (dI_t/dV_{tip}) at $V_{tip} = 0$ V. The $dI_t/dV_{tip}(0 \text{ V})$ values show a monotonic decrease for decreasing t and remain finite down to 1 uc. The red solid line indicates the $dI_t/dV_{tip}(0 \text{ V})$ value for a 50-uc film. Each curve is averaged over an area of 100 nm $\times$ 100 nm by a grid spectroscopic mode with 20×20 sampling pixels. All STS measurements were carried out at room temperature with the same tip under identical scanning conditions, namely, $I_t = 0.1$ nA and $V_{tip} = 0.5$ V.

remain, and the strongest peak moves toward E_F. In addition, the DOS at E_F, i.e., N_0, becomes larger. Using these DOS values, the T_C values were also estimated with Eq. (2), and these are plotted as red squares in Fig. 2(a).

The systematic variation of the DOS at E_F in the nonmagnetic states can be understood in terms of the orbital-selective QC effects. Note that the Ru^{4+} ion has four electrons in the t_{2g} orbitals, which are extended in the xy, yz, or zx planes. Because of the anisotropic shape of the t_{2g} orbitals, they can orient in a particular direction and provide directional hybridizations with surrounding oxygen ions. In bulk $SrRuO_3$, all of the t_{2g} orbitals form 2D networks of individual d_{xy}, d_{yz}, and d_{zx} orbitals by hybridizing with the oxygen $2p$ orbitals in each plane and form 2D tight-binding bands [25]. Figure 4(c) shows the schematic view of the Ru t_{2g} orbitals for the 1-uc sample. The (red) d_{xy} orbitals are extended in the xy plane, so the corresponding pDOS should have a 2D van Hove singularity, shown as the red-shaded area at the top of Fig. 4(b). On the other hand, the (blue) d_{yz} (or d_{zx}) orbitals should be extended in the yz (zx) plane, but they are truncated by the top and bottom interfaces. This QC effect in the d_{yz} and d_{zx} orbitals will result in a pDOS with strong 1D singularities near the band edges, shown as the blue-shaded area at the top of Fig. 4(b). Note that the pDOS for the 1-uc $SrRuO_3$ film determined from first-principles calculations can be explained as the sum of the pDOS for the d_{xy}, d_{yz}, and d_{zx} orbitals. A similar argument can be made for the 4-uc sample, as shown in Fig. 4(d). In this case, the resulting pDOS of the d_{yz} and d_{zx} orbitals should have eight peaks, shown in the blue-shaded area at the bottom of Fig. 4(b). The success of these simple arguments suggests that the calculated changes in the pDOS shown in Fig. 4(b) can be interpreted in terms of the orbital-selective QC effects.

The systematic change in pDOS of the $SrRuO_3$ films should also affect their magnetic properties. We calculated the pDOS for the $SrRuO_3$ films in ferromagnetic configurations, as shown in Fig. 4(e). For the thicker films, i.e., $t = 4$ and 3 uc, the calculations show that there is a large asymmetry in the pDOS between the spin-up and spin-down states, supporting the Stoner-type ferromagnetic ground state. The calculated values of the magnetic moment are 0.42 and $0.14 \mu_B$/Ru for $t = 4$ and 3 uc, respectively. On the other hand, for the thinner films, i.e., $t = 2$ and 1 uc, the nonmagnetic states are favored energetically. These predictions explain how T_C becomes zero for our $SrRuO_3$ sample with $t = 2$ uc.

In summary, we observed that the ferromagnetic Curie temperature of $SrRuO_3$ ultrathin films vanishes for the 2-unit-cell samples. Using *in situ* scanning tunneling spectroscopy and first-principles calculations, we showed that such a decrease might originate from a decrease in the density of states at the Fermi level, an effect due to orbital-selective quantum confinement effects. This work suggests that the properties of itinerant ferromagnetic materials can be controlled by geometric constriction at the nanoscale level.

*twnoh@snu.ac.kr
[1] G. Cao *et al.*, Phys. Rev. B **56**, 321 (1997).
[2] I. I. Mazin and D. J. Singh, Phys. Rev. B **56**, 2556 (1997).
[3] T. Moriya, *Spin Fluctuations in Itinerant Electron Magnetism* (Springer, Berlin, 1985).
[4] M. C. Tringides, M. Jalochowski, and E. Bauer, Phys. Today **60**, No. 4, 50 (2007).
[5] H. N. Lee *et al.*, Appl. Phys. Lett. **84**, 4107 (2004).
[6] M. Stengel and N. A. Spaldin, Nature (London) **443**, 679 (2006).
[7] S. C. Gausepohl *et al.*, Appl. Phys. Lett. **67**, 1313 (1995).
[8] K. S. Takahashi *et al.*, Phys. Rev. B **67**, 094413 (2003).
[9] T. Fujii *et al.*, Appl. Phys. Lett. **86**, 012107 (2005).
[10] C. H. Ahn, J. M. Triscone, and J. Mannhart, Nature (London) **424**, 1015 (2003).
[11] J. Junquera and P. Ghosez, Nature (London) **422**, 506 (2003).
[12] J. Y. Jo *et al.*, Phys. Rev. Lett. **97**, 247602 (2006).
[13] R. Ramesh and N. A. Spaldin, Nature Mater. **6**, 21 (2007).
[14] Y. J. Chang *et al.*, Phys. Rev. B **76**, 075118 (2007).
[15] J. C. Choi *et al.*, Appl. Phys. Lett. **79**, 1447 (2001).
[16] W. Hong *et al.*, Phys. Rev. Lett. **95**, 095501 (2005).
[17] D. Toyota *et al.*, Appl. Phys. Lett. **87**, 162508 (2005).
[18] J. Xia *et al.*, arXiv:0811.0384v1.
[19] J. M. Rondinelli *et al.*, Phys. Rev. B **78**, 155107 (2008).
[20] C. Kittel, *Introduction to Solid State Physics* (Wiley, New York, 1986).
[21] J. Okamoto *et al.*, Phys. Rev. B **60**, 2281 (1999).
[22] M. Shepard *et al.*, J. Appl. Phys. **81**, 4978 (1997).
[23] C. J. Chen, *Introduction to Scanning Tunneling Microscopy* (Oxford University Press, New York, 1993).
[24] Recently, it was pointed out that the properties of $SrRuO_3$ films grown by PLD would have significant amounts of ruthenium vacancies and that resulting disorder could affect transport properties and density of states around a 0–2 eV region near E_F. [Refer to W. Siemons *et al.*, Phys. Rev. B **76**, 075126 (2007)]; By comparing our experimental data with those for bulk $SrRuO_3$ [refer to L. Pi *et al.*, J. Phys. Condens. Matter **14**, 7391 (2002)]; and $SrTi_{1-x}Ru_xO_3$ films [K. W. Kim *et al.*, Phys. Rev. B **71**, 125104 (2005)], we found that the amount of such vacancies in our film should be quite small. Also, our films do not show the upturn of resistivity at low temperature down to 20 K, which is the hallmark of the weak localization, indicating that the disorder effect should play little role in the decrease of N_0.
[25] R. M. Martin, *Electronic Structure: Basic Theory and Practical Methods* (Cambridge University Press, Cambridge, England, 2004).